J. Water Environ. Nanotechnol., 5(4): 331-341 Autumn 2020

ORIGINAL RESEARCH PAPER

The MoS_2/S-Doped Graphitic Carbon Nitride: Synthesis and Application as a Composite for Removing Organic Pollutant

Mahdieh Chegeni*, Mokhgan mehri, Mehdi Hosseini

[1] *Department of Chemistry, Faculty of Science, Ayatollah Boroujerdi University, Boroujerd, 69199-69737 Iran.*

Received: 2020-09-02 Accepted: 2020-10-09 Published: 2020-11-15

ABSTRACT

The MoS_2/S-doped graphitic carbon nitride (MoS_2/S-g-C_3N_4) was synthesized by a simple method and applied for methylene blue (MB) removal as an organic pollutant. The structure of MoS_2/S-doped graphitic carbon nitride was characterized using FTIR, XRD, SEM, TGA, and BET techniques. The accomplishment of MoS_2/S-doped graphitic carbon nitride as an adsorbent was investigated for the removal of MB from an aqueous solution. The various parameters were studied such as pH, initial MB concentration, adsorbent dose, temperature, and time. The best findings were obtained at pH=8, 8 ppm MB concentration, 0.05 g MoS_2/S-g-C_3N_4, 30 min, and 22 ˚C. The Langmuir isotherm model was adopted with the obtained data. The kinetic studies have indicated that the adsorption of methylene blue could be well described by the second-order equation. Maximum adsorption was calculated as 166 mg/g. The degradation of MB was studied by MoS_2/S-doped graphitic carbon nitride under Light Emission Diode (LED). Results showed that the MoS_2/S-doped graphitic carbon nitride could enhance the photocatalytic activity compared to pure g-C_3N_4 and MoS_2/g-C_3N_4. The findings confirmed that the MoS_2/S-doped graphitic carbon nitride could be applied as an efficient, low-cost adsorbent, and photocatalyst in order to remove cationic dyes such as methylene blue.

Keywords: *MoS_2/S-doped graphitic carbon nitride, adsorption, methylene blue, degradation*

How to cite this article

Chegeni M., mehri M., Hosseini M. The MoS_2/S-Doped Graphitic Carbon Nitride: Synthesis and Application as a Composite for Removing Organic Pollutant . J. Water Environ. Nanotechnol., 2020; 5(4): 331-341.

DOI: 10.22090/jwent.2020.04.004

INTRODUCTION

In recent years, some factories such as food, textile, and pharmaceutical could affect human health and lead to important damages. In effluents from industries, synthetic organic dyes have an important role in the ecosystem, due to their biotoxicity property. There are various methods to overcome this problem including chemical oxidation [1], electrochemical process [1], biological system [2], and adsorption [3]. One of the effective methods to remove dyes is adsorption, due to low cost, easy performance, and high yield. Some of the adsorbents could be used in order to remove hazardous material including peptide fibrils [4], porous graphene oxide/alkali lignin aerogel [5], $WO_{2.72}$ nanowires [6], activated carbon (AC) metal-organic frameworks [7], and perlite [8] but many of them have difficult preparation procedures, inexpensive starting materials and lack of ability to remove organic pollutants. Further treatment is a significant disadvantage of the adsorbents since, in the adsorption mechanism, pollutants only can transfer between solid and aqueous phases, therefore dyes cannot be degraded and eliminated environmentally.

Nowadays, the photocatalyst procedures apply for the degradation of hazardous material

* Corresponding Author Email: *mahdieh.chegeni@abru.ac.ir*

frequently. This procedure could decompose toxic pollutants. To achieve this purpose, various semiconductor could be used as a photocatalyst. In environmental subjects, adsorption and photocatalytic procedure could result from unique properties in order to remove organic contaminants. Some of bifunctional materials could be used to remove dyes including TiO_2/biochar [9], MgO/TiO_2 [10], ZnO/AC [11], g-C_3N_4/biochar [12]. It is an important subject that materials have adsorption and photocatalyst activities together but many of these compounds have one of these properties individually, subsequently, it is necessary to synthesis the composite with both adsorption and photocatalytic effects.

In order to achieve high efficiency in the removal of organic waste, graphitic carbon nitride (g-C_3N_4) was introduced as a fascinating polymer in order to remove hazardous pollutants [13], reduce CO_2, produce H_2 [13], split water [14], and inactivate bacteria [15]. The photocatalytic performance of g-C_3N_4 could be limited by its bandgap, therefore to overcome this problem, various strategies could be used such as doping [16], heterostructure construction [17], and nanosheet formation [18].

Among these methods, the heterostructure formation including g-C_3N_4-based conventional type II, Z-scheme, and p–n heterostructure were used frequently. The direct Z-scheme heterostructure synthesis could be used as a useful modification procedure, due to its easy preparation and high efficiency [18]. One of the cationic dyes is methylene blue (MB) that could affect human health. Many kinds of literature were discussed about this compound but few of them were provided the degradation and adsorption of MB.

In this regard, we have used atom doping and direct heterostructure in order to improve g-C_3N_4 properties to obtain high efficiency. Our work in this article includes: 1) synthesis of MoS_2/S-g-C_3N_4; 2) characterization of MoS_2/S-g-C_3N_4; 3) application of this composite in order to remove methylene blue.

EXPERIMENTAL

Materials

Melamine, molybdenum disulfide (MoS_2), sulfuric acid (H_2SO_4), hydrochloric acid (HCl), sodium hydroxide (NaOH), methylene blue (MB), benzoquinone (BZQ), ammonium oxalate (AO), isopropanol (IPA), and ethanol were purchased from Merck and Aldrich companies.

Instruments

The Unicam-Galaxy 5000 was used to obtain the infrared absorption spectra. The X-Ray Diffraction (XRD) data were obtained by a Panalytical Xpertpro diffractometer using Cu Kα radiation (λ = 1.54178 Å). The Scanning Electron Microscope (SEM) was obtained by a Tescan Mira3-Lmu Microscope. The Brunauer–Emmett–Teller (BET) of the sample was recorded by nitrogen adsorption in a Belsorp Mini II apparatus. The photodegradation tests were carried out under 5 W LED lamps (450 nm). Thermogravimetric analysis (TGA) was obtained using Q600-TA (Unit State, 25 °C to 600 °C, N_2-atmosphere, a constant heating rate of 20 °C/min).

Preparation of MoS_2/S-doped graphitic carbon nitride

The S-g-C_3N_4 was prepared by melamine and sulfuric acid (2 % v/v) according to Ref [19]. The obtained product was calcinated by adding 0.4 g MoS_2 at 550 °C for 1 h at a heating rate of 5 °C/min. The MoS_2/S-graphitic carbon nitride was obtained and characterized by FTIR, SEM, XRD, and BET techniques.

Adsorption experiments

The adsorption condition including pH (2-12), the amounts of methylene blue (MB) (2-22 ppm), MoS_2/S-g-C_3N_4 dosage (0.002-0.15), contact time (10-420 min), and temperature (15-45 ˚C) were studied. The optimum conditions were obtained for the adsorption of MB on MoS_2/S-g-C_3N_4 and Table 1 has shown the condition of each experiment. The solution was analyzed on UV–vis spectrophotometer (665 nm), then adsorption capacity and % recovery were calculated by *Eqs* (1-2).

$$q_e = \frac{(c_i - c_e)V}{m} \quad (1)$$

$$R_e = \frac{(c_i - c_e)}{c_i} * 100 \quad (2)$$

The pH test (1): The Auta and Hameed method was used to obtain a point of zero charges (pHpzc) [13]. The pH of the solution was adjusted in the range from 2.0 to 12.0 using 0.1M of NaOH and HCl solutions. The experiment was carried out under the conditions of Table 1. After each test, the solution was centrifuged and analyzed using UV-Vis spectroscopy at 665 nm.

The adsorbent amount test (2): The optimal

Table 1. The conditions of MB adsorption on MoS_2/S-g-C_3N_4.

Test	pH	Dosage of adsorbent (g)	Initial MB concentration (ppm)	Time (min)	Temperature (°C)
1	2-12	0.05	10	120	25
2	8	0.005-0.15	10	120	25
3	8	0.05	2-22	120	25
4	8	0.05	8	60	25
5	8	0.05	8	60	22

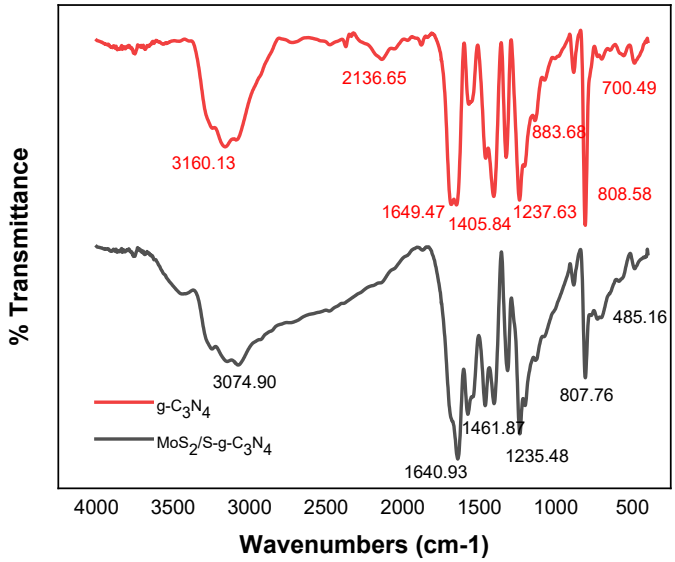

Fig. 1. FT-IR spectra of the g-C_3N_4 nanosheet and MoS_2/S- g-C_3N_4.

adsorbent amount was studied in the range of (0.002-0.15) that the conditions of tests are seen in Table 1. The samples were centrifuged and analyzed by UV-Vis spectrophotometer, and the concentration of MB was determined by *Eqs* (1-2).

The MB concentration test (3): Under the specified conditions (Table 1), the best MB concentration was obtained in the range of 2-22 ppm.

The optimum time test (4): The effect of time was investigated for the adsorption of MB on MoS_2/S-g-C_3N_4 (the range of 10-420 min, Table 1) and the results were calculated by *Eqs* (1-2).

The optimum temperature test (5): The temperature effect was studied in order to remove MB by MoS_2/S-g-C_3N_4 in the range of 15-45°C under specific conditions (Table 1).

In this study, the Langmuir and Freundlich isotherms *Eqs* (3,4) were used to explain the interaction mechanism between the adsorbent–adsorbate system at equilibrium [20,21].

$$ln\, q_e = \ln K_f + 1/n\, ln C_e \quad (3)$$

$$\frac{C_e}{q_e} = \frac{1}{q_{max}\, b} + \frac{C_e}{q_{max}} \quad (4)$$

To explain the kinetic models, the pseudo-first-order and pseudo-second-order equations were used to describe the interaction between MB and MoS_2/S-g-C_3N_4 (Eqs (5,6)) [22,23].

$$\ln\left(q_e - q_t\right) = lnq_e - k_1 t \quad (5)$$

$$\frac{t}{q_t} = \frac{1}{k_2\, q_e^2} + \frac{t}{q_e} \quad (6)$$

RESULTS AND DISCUSSION

Characterization of MoS_2/S-g-C_3N_4

The FT-IR spectra were used to confirm the formation of g-C_3N_4 and MoS_2/S-g-C_3N_4 (Fig. 1). The breathing mode of tri-S-azine units is

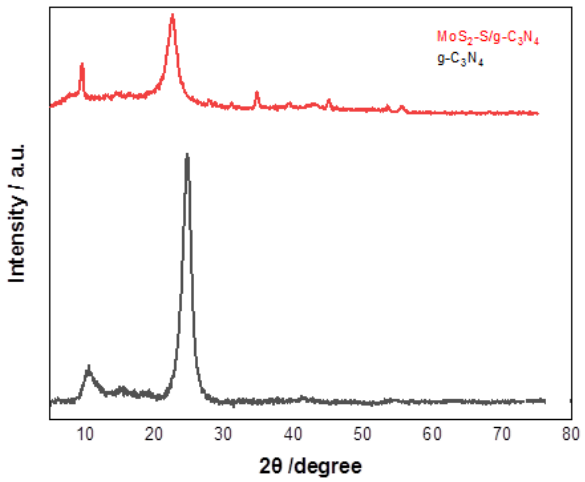

Fig. 2. XRD patterns of the bulk g-C_3N_4 and MoS_2/S-g-C_3N_4.

determined at 807-808 cm^{-1} in both spectra. The stretching peaks of aromatic C–N heterocycles in g-C_3N_4 can be determined by the peaks at 1237 cm^{-1}, 1405 cm^{-1}, and 1649 cm^{-1}. The absorption peak at 2136 cm^{-1} belongs to multiple C–C bonds. The N–H and O–H vibrations are ascribed at 3000-3400 cm^{-1} as a broad peak. The stretching model of the doping atom can be observed in the FT-IR spectrum of MoS_2/S-g-C_3N_4. The sulfur vibrations are seen in the range of 1000-1200 cm^{-1}. The Mo-S peak is shown by a weak peak around at 485 cm^{-1} in nanocomposite [24]. These spectra suggest that doping on g-C_3N_4 changed the original structure slightly and the framework of g-C_3N_4 was not disturbed.

The crystal structure of bulk g-C_3N_4 and MoS_2/S-doped graphitic carbon nitride is shown in Fig. 2. The XRD pattern of bulk g-C_3N_4 shows two obvious peaks at 2Θ=27.66˚ and 2Θ=13.19˚, that corresponds to the (100) and (002) planes of interlayer stacking conjugated aromatic in g-C_3N_4 (JCPSD: 98-002-6302). In X-ray diffraction of MoS_2/S- g-C_3N_4, the pick at 2Θ=27.59° belongs to (002) planes of the aromatic system. The main peak for g-C_3N_4 is seen with higher intensity than for MoS_2/S- g-C_3N_4 and it is shifted to low angles in nanocomposite (2Θ=27.66˚ in contrast to 27.59°), due to the substitution of the lattice atoms in carbon nitride with S and MoS_2. The broadening of diffraction peaks also is observed, due to a decrease in crystal size and nano-sized material that can suggest the increasing surface area and as a potential for efficient adsorption [25]. The peaks at 2Θ=39.65˚, 60.56 ˚, and 76.17˚ can respectively be indexed to the standard value (JCPSD: 98-002-6302) that it possesses the loading of S and MoS_2 in the g-C_3N_4 with 55 nm average crystallite size.

In Fig. 3, the nitrogen adsorption-desorption and BET isotherms of MoS_2/S-g-C_3N_4 are shown. These plots belong to type IV isotherms according to IUPAC classification. The hysteresis loop region presents mesopores in the MoS_2/S-g-C_3N_4. The mean pore diameter of MoS_2/S-g-C_3N_4 was obtained at 31.22 nm, also a BET analysis showed that the specific surface and total pore volume is 33.52 m^2/g and 0.11 $cm^3\ g^{-1}$. The formation of MoS_2/S-g-C_3N_4 is characterized by a higher value of specific surface area (33.52 m^2/g) compared to bulk g-C_3N_4 (25 m^2/g).

In Fig. 4, the scanning electron microscopy images of pure C_3N_4 and MoS_2/S-g-C_3N_4 are seen. Figs. 4a, b, illustrate that pure C_3N_4 has a structure like graphite with a big aggregation, smooth and sheet-like morphology, and non-uniform dimensions. The formation of MoS_2/S-g-C_3N_4 can be seen from Figs. 4c,d, that several MoS_2 and S atoms were loaded or firmly deposited on the pure g-C_3N_4 surfaces in the range of 16-31 nm.

As shown in Fig. 5, the TGA analysis was applied to study the thermal stability of MoS_2/S-g-C_3N_4. In the first step, weight loss was accrued around 100 ˚C, due to the evaporation of physisorbed water, second step weight loss was shown between 380-420 ˚C due to the degradation of g-C_3N_4 and oxidation of MoS_2. It is indicated that 40 % weight loss of nanocomposite at 25 °C to 600 °C compared

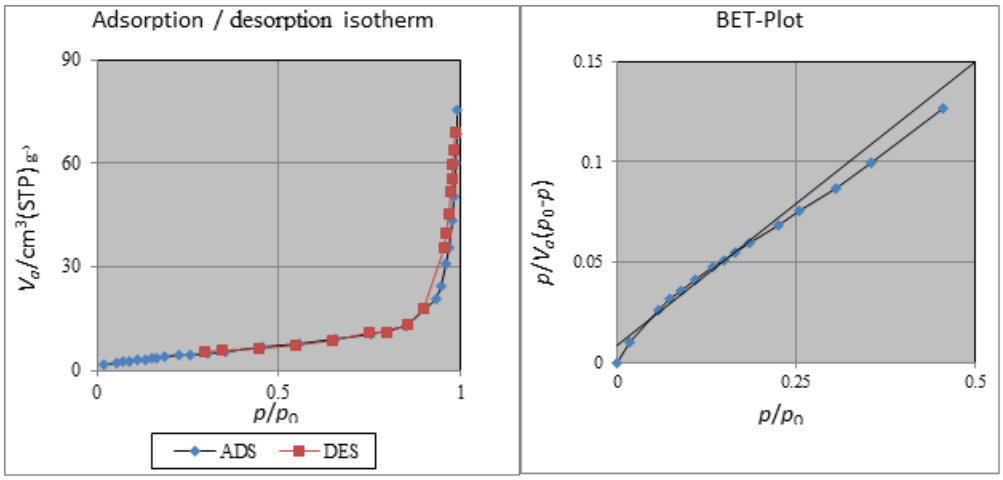

Fig. 3. Nitrogen adsorption–desorption and BET plots of the MoS_2/S-g-C_3N_4.

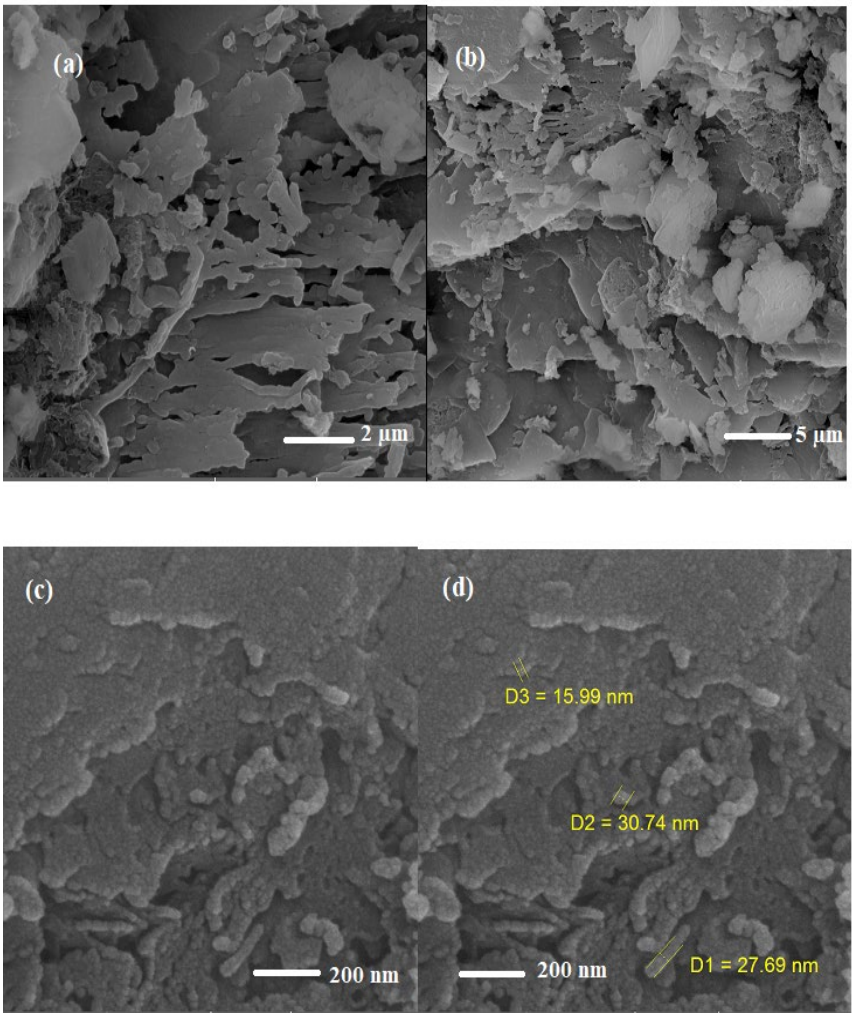

Fig. 4. SEM images of the (a,b) bulk g-C_3N_4 and (c,d) MoS_2/S-g-C_3N_4.

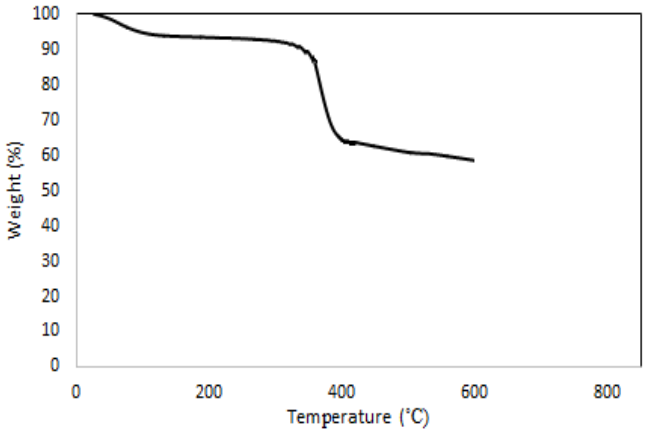

Fig. 5. TGA curves of MoS_2/S-g-C_3N_4.

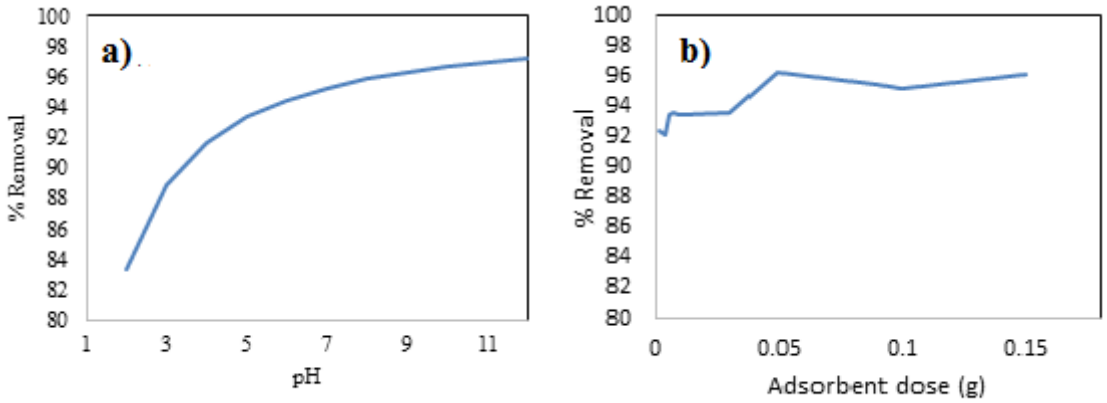

Fig. 6. The effect of (a) pH and (b) adsorbent dose for MB adsorption on MoS_2/S-g-C_3N_4.

to the findings could be confirmed the thermal stability of nanocomposite.

Batch adsorption studies

In this study, the effect of solution parameters such as pH, adsorbent doses, (MB) quantities, contact time, and temperature for the adsorption on MoS_2/S-g-C_3N_4 was investigated.

The ionization solution can play an important role in the adsorption of MB on MoS_2/S-g-C_3N_4.

Several solution pHs can be influenced by the surface charge of adsorbent because it can be protonated and deprotonated by hydrogen and hydroxide ions. The adsorption of adsorbent can be changed, therefore the pH of the solution is a significant factor for the removal of MB. In this study, the pHpzc was determined 7.5 that it is evidenced that the pH surface of nanocomposite is positive when the media pH is lower than pHpzc and it was negative at pH higher than pHpzc. The pH was varied from (2-12) and other parameters were kept constant, according to Table 1. The best efficiency was seen at alkaline pH (pH=8), due to interaction between the positive charge of MB and the negative surface of MoS_2/S-g-C_3N_4 (Fig. 6a). It can see that the adsorption of MB on MoS_2/S-g-C_3N_4 was decreased at low pH because of the electrostatic repulsion between the MB as a cationic dye and the hydrogen ion concentration in the solution, also electrostatic interaction between negatively charged groups and MB can be helped to high removal efficiency at high value of pH.

The effect of adsorbent dosage was studied to obtain the best amount of MoS_2/S-g-C_3N_4. As shown in Fig. 6b, the recovery efficiency is increased when the MoS_2/S-g-C_3N_4 amount was reached to 0.05 g,

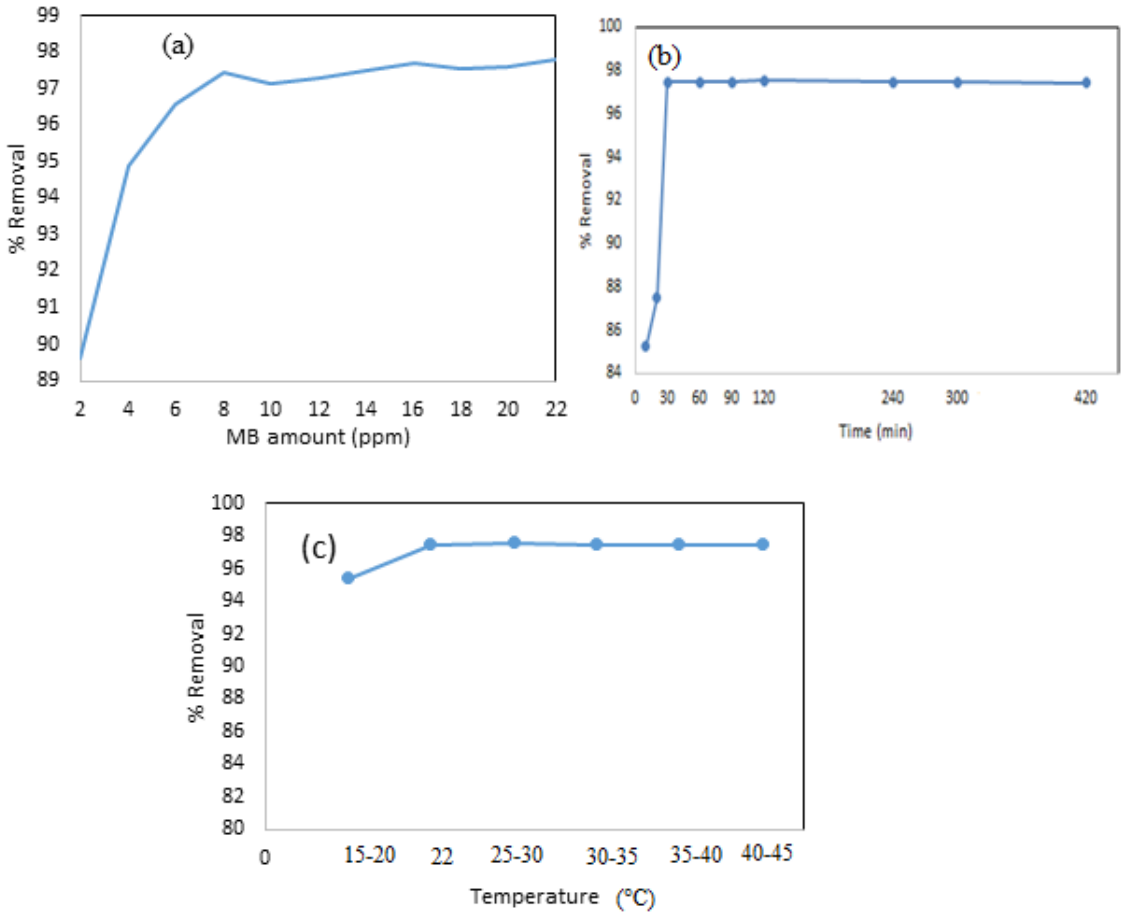

Fig. 7. The effect of (a) MB amount, (b) time and (c) temperature for the MB adsorption and MoS_2/S-g-C_3N_4.

because the increasing adsorbent surface resulted in high interaction between the MB and MoS_2/S-g-C_3N_4. By increasing the amount of adsorbent, the % efficiency was constant because the initial concentration of MB was unchanged.

The effect of MB dosage was obtained according to Fig. 7a. The maximum removal was determined at 8 ppm. The initial MB amount was a driving force in the adsorption process. At high MB concentrations, the adsorption efficiency was decreased, due to the presence of excess MB in the reaction mixture.

Another important parameter in the adsorption process is time. To complete the MB adsorption on MoS_2/S-g-C_3N_4, the effect of time was studied on this process. After the beginning adsorption, the removal rate is maximized at 30 min (Fig. 7b). It was shown the % removal was increased with increasing contact time. After 30 min, the adsorption efficiency was not a significant change, due to the adsorbent sites became saturated.

Next section, the effect of temperature was considered to obtain % removal. It was found that the temperature change had little impact on the adsorption process. The percentage removal rate was achieved a high value at 22 °C (Fig. 7c). With further increase in temperature, the presence of a vacant site inside the pores was almost filled and the removal efficiency remains constant.

For designing the real wastewater, the Langmuir and Freundlich isotherms models were applied to the evaluation of experimental data. Regression coefficients ($\mathbf{R^2}$) are exposed to a high value in the Langmuir model compared to Freundlich isotherm. The constants of the isotherm models are shown in Table 2. These results were obtained by the plots from **Eqs**. 3-4, therefore the maximum adsorption capacity was achieved by the slope of the plot from **Eq**. 4. It can be suggested that the adsorption process might be heterogeneous and

Table 2. Information of isotherm models for MB adsorption on MoS_2/S-g-C_3N_4.

Freundlich			Langmuir		
K_f (mg/L)	n	R^2	q_{max} (mg/g)	K_l (L/mg)	R^2
0.001	0.57	0.94	166	0.07	0.97

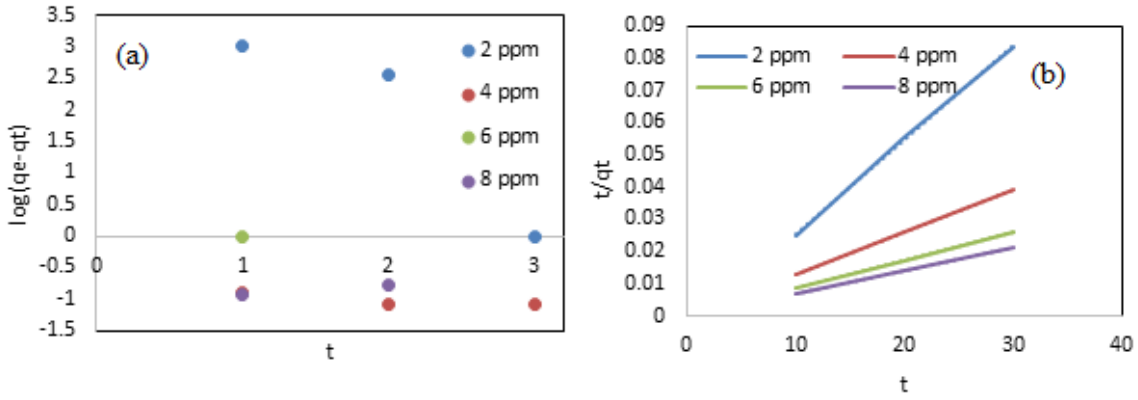

Fig. 8. (a) Pseudo-second-order kinetics, and (b) pseudo-first-order kinetics of MB adsorption on MoS_2/S-g-C_3N_4.

mono-layer.

One of the important factors for the evaluation of an adsorbent is the study of adsorption kinetics. The pseudo-first-order and pseudo-second-order models were used to discuss the affinity between MB adsorption on MoS_2/S-g-C_3N_4. The graph plotted between t/q_t and time is depicted in a pseudo-second-order model that is shown in Fig. 8a. A graph plotted between $log\ (q_e\text{-}q_t)$ and time is seen in Fig. 8b. The obtained data of adsorption kinetics were adopted by the pseudo-second-order model, it can be seen that the correlation coefficient R^2 was fitted to this model, due to a higher value than another model.

Photocatalytic and adsorption studies for MB

The degradation of MB was monitored by measuring the absorbance amount using a double beam UV– Vis spectrophotometer at 665 nm under the Light Emitting Diode (LED) condition. The amount of MB was calculated, the result was shown 98% degradation rather to dark condition.

In the dark, the nanocomposite acted as an adsorbent, then under LED condition, can be degraded MB as a photocatalyst. Also, the color of the MB aqueous solution was changed gradually, the surface of the nanocomposite was covered with particles, and they blocked the surface of the adsorbent to absorbed light. Therefore, MoS_2/S-g-C_3N_4 had both adsorption and photocatalytic activities.

In this regard, the adsorption yield at ambient conditions and photocatalytic efficiency are near together. When both of these activities were combined, the water purification can be improved. Adsorption activity can be separated MB and it was moved to another phase but photocatalytic activity can be degraded. To the evidence of this activity, the photocatalytic test was carried out.

In the photocatalytic mechanism, the first photocatalyst was absorbed photon, next step the photo photogenerated electrons were transferred to the surface of photocatalyst, then the pollutant was reacted to photogenerated electrons and holes. The pollutants can be oxidized to the CO_2 and H_2O molecules by h^+, $\bullet O^{2-}$, and •OH species. The benzoquinone (BZQ), ammonium oxalate (AO), and isopropanol (IPA) can quench active species. The $\bullet O^{2-}$, h^+ and •OH species were affected on MB degradation, as shown in Fig. 9. According to results, by adding BZQ, AO, and IPA, the yield of MB degradation was decreased to 75 %, 81 %, and 69 %. It can be evidenced that the active species affected MB removal [19, 26-27].

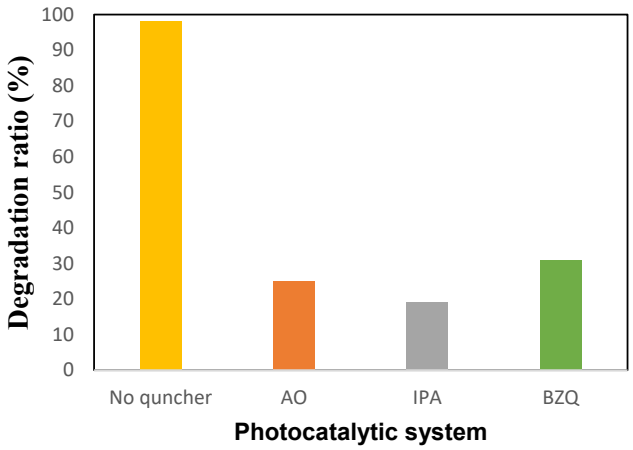

Fig. 9. The corresponding degradation ratio of MB on MoS_2/S-g-C_3N_4 under LED irradiation.

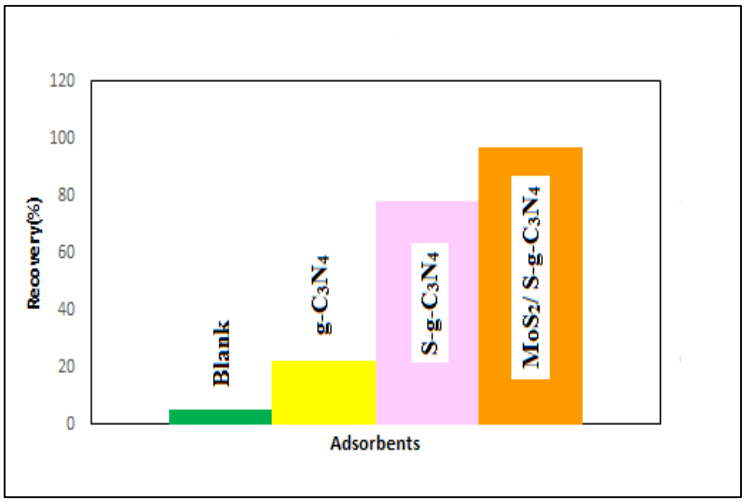

Fig. 10. Effect of adsorbent type on MB adsorption.

Table 3. Comparison of MB removal for various adsorbents.

Adsorbent	Pollutant	Removal (%)	Degradation	Adsorption	Reference
Metal organic framework	MB	98.67%	-	-	[28]
$MnFe_2O_4$@CS-SiO_2 microsphere	MB	93.86%	-	-	[29]
Mesoporous titania (TiO_2) – poly vinyl alcohol (PVA)	MB	97.1%	-	-	[30]
Bentonite	MB	70 %	-	-	[31]
$NiFe_2O_4$/Ag_3PO_4	MB	79.41%	+	+	[32]
MoS_2/S-g-C_3N_4	MB	98 %	+	+	In this work

In other studies, the adsorption ability of g-C_3N_4, S-g-C_3N_4, and MoS_2/S-g-C_3N_4 was investigated that the findings can be seen in Fig. 10. It is obvious that adsorption activity was increased when MoS_2 was added to S-g-C_3N_4.

The comparison of MoS_2/S-g-C_3N_4 and other

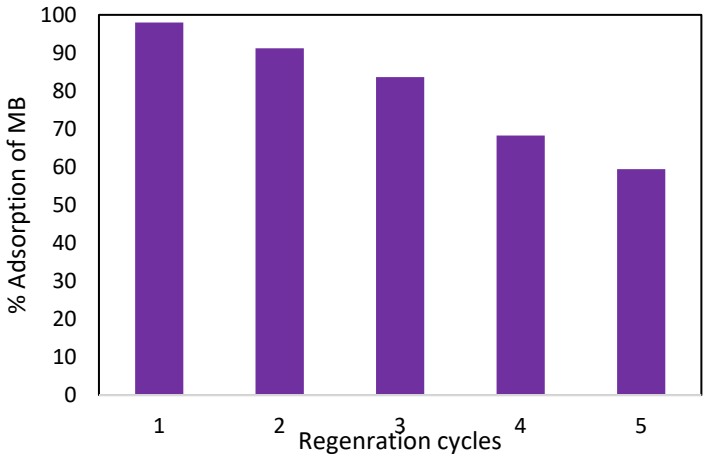

Fig. 11. Recycling study

adsorbents can be seen in Table 3. The findings show the ability of MoS_2/S-g-C_3N_4 to remove MB compared to other literature. Many of them only can be adsorbed not omitted pollutant, therefore the advantage of MoS_2/S-g-C_3N_4 is degradation and adsorption activities.

Recyclability

The recyclability of adsorbent is an important subject due to its effect on costs. After adsorption of MB from aqueous solution, the MoS_2/S-g-C_3N_4 can be recovered in ethanol solution (% 60 *v/v*). The results were shown the excellent reusability of MoS_2/S-g-C_3N_4 after 5 cycles (Fig. 11). It can be evidenced that a good and environmentally friendly compound for the purification of MB wastewater.

CONCLUSION

The MoS_2/S-g-C_3N_4 can be used as an efficient composite for the adsorption and degradation of MB. The removal of MB by MoS_2/S-g-C_3N_4 was depended on pH, MB concentration, MoS_2/ S-g-C_3N_4, time, and temperature. The isotherm and kinetic studies were fitted by Langmuir and Pseudo-second-order kinetics. The present findings illustrated that MoS_2/ S-g-C_3N_4 can be degraded MB under LED condition. FT-IR, XRD, SEM, BET, TGA analysis, and adsorption tests introduced the MoS_2/ S-g-C_3N_4 as an efficient and green composite to the removal of MB compared to non-doping starting materials.

CONFLICT OF INTEREST

The authors declare that they have no conflict of interest.

REFERENCES

1. Liang J, Xia X, Zaman WQ, Zhang W, Lin K, Hu S, et al. Bioaccumulation and toxic effects of decabromodiphenyl ether in the presence of nanoscale zero-valent iron in an earthworm–soil system. Chemosphere. 2017;169:78-88.
2. Vörösmarty CJ, McIntyre PB, Gessner MO, Dudgeon D, Prusevich A, Green P, et al. Global threats to human water security and river biodiversity. Nature. 2010;467(7315):555-61.
3. Ighalo JO, Adeniyi AG. Adsorption of pollutants by plant bark derived adsorbents: An empirical review. Journal of Water Process Engineering. 2020;35:101228.
4. Brar SK, Wangoo N, Sharma RK. Enhanced and selective adsorption of cationic dyes using novel biocompatible self-assembled peptide fibrils. Journal of Environmental Management. 2020;255:109804.
5. Wu Z, Huang W, Shan X, Li Z. Preparation of a porous graphene oxide/alkali lignin aerogel composite and its adsorption properties for methylene blue. International Journal of Biological Macromolecules. 2020;143:325-33.
6. Shang Y, Cui Y, Shi R, Yang P, Wang J, Wang Y. Regenerated WO2.72 nanowires with superb fast and selective adsorption for cationic dye: Kinetics, isotherm, thermodynamics, mechanism. Journal of Hazardous Materials. 2019;379:120834.
7. Hasanzadeh M, Simchi A, Shahriyari Far H. Nanoporous composites of activated carbon-metal organic frameworks for organic dye adsorption: Synthesis, adsorption mechanism and kinetics studies. Journal of Industrial and Engineering Chemistry. 2020;81:405-14.
8. Mathialagan T, Viraraghavan T. Adsorption of cadmium from aqueous solutions by perlite. Journal of Hazardous Materials. 2002;94(3):291-303.
9. Khataee A, Kayan B, Gholami P, Kalderis D, Akay S. Sonocatalytic degradation of an anthraquinone dye using TiO2-biochar nanocomposite. Ultrasonics Sonochemistry. 2017;39:120-8.
10. Jia Y, Yu X-Y, Luo T, Jin Z, Sun B, Liu J-H, et al. Necklace-

like mesoporous MgO/TiO2heterojunction structures with excellent capability for water treatment. Dalton Trans. 2014;43(6):2348-51.
11. Sobana N, Swaminathan M. Combination effect of ZnO and activated carbon for solar assisted photocatalytic degradation of Direct Blue 53. Solar Energy Materials and Solar Cells. 2007;91(8):727-34.
12. Zhang J, Mao X, Xiao W, Zhuang Y. Photocatalytic degradation of sulfamethazine by graphitic carbon nitride-modified zinc molybdate: Effects of synthesis method on performance, degradation kinetics, and mechanism. Chinese Journal of Catalysis. 2017;38(12):2009-20.
13. Kong L, Wang J, Ma F, Sun M, Quan J. Graphitic carbon nitride nanostructures: Catalysis. Applied Materials Today. 2019;16:388-424.
14. Wang S, Chen L, Zhao X, Zhang J, Ao Z, Liu W, et al. Efficient photocatalytic overall water splitting on metal-free 1D SWCNT/2D ultrathin C3N4 heterojunctions via novel non-resonant plasmonic effect. Applied Catalysis B: Environmental. 2020;278:119312.
15. Zhang C, Li Y, Shuai D, Shen Y, Xiong W, Wang L. Graphitic carbon nitride (g-C3N4)-based photocatalysts for water disinfection and microbial control: A review. Chemosphere. 2019;214:462-79.
16. Jourshabani M, Lee B-K, Shariatinia Z. From Traditional Strategies to Z-scheme Configuration in Graphitic Carbon Nitride Photocatalysts: Recent Progress and Future Challenges. Applied Catalysis B: Environmental. 2020;276:119157.
17. Xiong M, Rong Q, Meng H-m, Zhang X-b. Two-dimensional graphitic carbon nitride nanosheets for biosensing applications. Biosensors and Bioelectronics. 2017;89:212-23.
18. Fu J, Yu J, Jiang C, Cheng B. g-C3N4-Based Heterostructured Photocatalysts. Advanced Energy Materials. 2017;8(3):1701503.
19. Chegeni M, Goudarzi F, Soleymani M. Synthesis, Characterization and Application of V 2 O 5 /S-Doped Graphitic Carbon Nitride Nanocomposite for Removing of Organic Pollutants. ChemistrySelect. 2019;4(46):13736-45.
20.Van der Bruggen B, Freundlich Isotherm., In Encyclopedia of Membranes. In pringer Berlin Heidelberg: Berlin, Heidelberg, Drioli, E. G., L. Ed. 2015; 25-60.
21. Langmuir I. THE ADSORPTION OF GASES ON PLANE SURFACES OF GLASS, MICA AND PLATINUM. Journal of the American Chemical Society. 1918;40(9):1361-403.
22.Lagergren S. About the theory of so-called adsorption of soluble substances. Kungliga Svenska Vetenskapsakademiens Handlingar 1898;24:1-39.
23. Ho YS, McKay G. The kinetics of sorption of divalent metal ions onto sphagnum moss peat. Water Research. 2000;34:735-742.\
24. Yu J, Wang S, Cheng B, Lin Z, Huang F. Noble metal-free Ni(OH)2–g-C3N4 composite photocatalyst with enhanced visible-light photocatalytic H2-production activity. Catalysis Science & Technology. 2013;3(7):1782.
25. Li D, Song H, Meng X, Shen T, Sun J, Han W, et al. Effects of Particle Size on the Structure and Photocatalytic Performance by Alkali-Treated TiO2. Nanomaterials. 2020;10(3):546.
26. Xiao Y, Wang T, Qiu G, Zhang K, Xue C, Li B. Synthesis of EDTA-bridged CdS/g-C3N4 heterostructure photocatalyst with enhanced performance for photoredox reactions. Journal of Colloid and Interface Science. 2020;577:459-70.
27. Mo Z, Xu H, Chen Z, She X, Song Y, Lian J, et al. Construction of MnO2/Monolayer g-C3N4 with Mn vacancies for Z-scheme overall water splitting. Applied Catalysis B: Environmental. 2019;241:452-60.
28. I M, Saleh HAM, Qasem KMA, Shahid M, Mehtab M, Ahmad M. Efficient and selective adsorption and separation of methylene blue (MB) from mixture of dyes in aqueous environment employing a Cu(II) based metal organic framework. Inorganica Chimica Acta. 2020;511:119787.
29. Liu Z, Chen G, Hu F, Li X. Synthesis of mesoporous magnetic MnFe2O4@CS-SiO2 microsphere and its adsorption performance of Zn2+ and MB studies. Journal of Environmental Management. 2020;263:110377.
30. Jaseela PK, Garvasis J, Joseph A. Selective adsorption of methylene blue (MB) dye from aqueous mixture of MB and methyl orange (MO) using mesoporous titania (TiO2) – poly vinyl alcohol (PVA) nanocomposite. Journal of Molecular Liquids. 2019;286:110908.
31. Momina, Mohammad S, Suzylawati I. Study of the adsorption/desorption of MB dye solution using bentonite adsorbent coating. Journal of Water Process Engineering. 2020;34:101155.
32. Zhao G-y, Liu L-j, Li J-r, Liu Q. Efficient removal of dye MB: Through the combined action of adsorption and photodegradation from NiFe2O4/Ag3PO4. Journal of Alloys and Compounds. 2016;664:169-74.